THE JOURNAL OF PHYSICAL CHEMISTRY C

pubs.acs.org/JPCC Article

Vibrational Sum Frequency Scattering in Absorptive Media: A Theoretical Case Study of Nano-objects in Water

Sergey Kulik, Saranya Pullanchery, and Sylvie Roke*

Cite This: https://dx.doi.org/10.1021/acs.jpcc.0c05196 Read Online

ACCESS | Metrics & More | Article Recommendations | Supporting Information

ABSTRACT: The structures of interfaces of nano- and microscale objects in an aqueous solution are important for a wide variety of physical, chemical, and biological processes. Vibrational sum frequency (SF) scattering has emerged as a useful and unique probe of the interfacial structure of nano- and microscale objects in water. However, the full surface vibrational stretch mode spectrum has not been measured yet, even though it would be extremely informative to do so. The reason for this is that probing the vibrational modes of interfacial water requires a full understanding of how the linear absorptive properties of the bulk aqueous medium influence the SF scattering process. Here, we have simulated vibrational SF scattering spectra of the interface of nanoscale objects dispersed in water. We analyzed the effect of the infrared pulse absorption on the outcome of surface vibrational SF scattering measurements. We find that both infrared absorption as well as the type of optical detection can drastically modify the measured vibrational interfacial spectrum. The observed changes comprise spectral distortion, frequency shifting of the main vibrational stretch mode, and the introduction of a new high-frequency peak. This last feature is enhanced by nonresonant interactions.

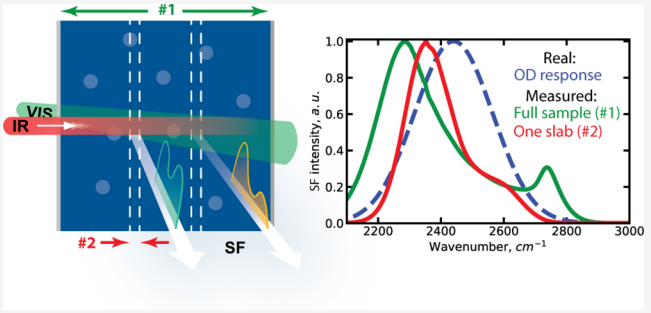

INTRODUCTION

Aqueous interfaces are abundant in nature and important for a host of processes related to atmospheric,[1,2] chemical,[3] biological,[4] and geological[5] transformations. The molecular and structural properties of aqueous interfaces are therefore important. Measuring these is challenging, as one has to separate the probed properties of the small minority of interfacial water molecules from the very large amount of bulk water in a typical sample. The demonstration of surface vibrational sum frequency generation (SFG) spectroscopy[6,7] therefore represented a great improvement as it allowed the selective spectroscopic identification of interfacial water in a background-free way. Since then, vibrational SFG has been used in reflection geometry to probe planar extended interfaces of water and salt solutions in contact with air,[8−14] lipids,[15−20] liquids,[21−24] polymers,[25−28] proteins,[29] quartz and silica,[30−33] metals,[34−36] and many others (see, e.g., further reviews in Refs.[37−44]).

The next step in understanding the complexity of aqueous interfaces is to probe realistic nano- and microscale sized interfaces rather than a planar extended model interface, as shape, size, and environment influence the molecular and macroscopic properties of a system. To do so, vibrational sum frequency scattering (SFS)[45,46] was invented. Instead of reflecting infrared (IR) and visible (VIS) laser pulses from a planar extended interface, both beams are passed through a sample (Figure 1a), typically a liquid that contains particles, droplets or liposomes, and the interfacially generated sum frequency (SF) photons are scattered and detected. In this way, the interfaces of small objects in the size range of ∼20 nm−50 μm can be probed on a molecular level. While the surface vibrational spectrum provides information on the molecular species and the local environment, the scattering pattern as detected in different polarization combinations provides additional information on molecular orientation,[47] surface electrostatics,[48,49] aggregation,[50] and chirality.[51] Vibrational SFS spectra have been recorded in many spectral ranges, starting with probing C−H modes (from stearyl-coated silica particles in CCl_4 or other hydrophobic liquids[52,53]) as this is typically the sweet spot of the ultrafast infrared laser source that was used. Spectra were soon recorded of diverse objects in aqueous solution addressing a wider spectral range that contains vibrational C−H stretching,[54−56] bending,[57] amide bands,[57] P−O stretching,[58] −CN stretching,[59] S−O stretching,[54] and other modes. The surface vibrational spectrum of water was measured by SFS in the form of heavy water droplets

Received: June 8, 2020
Revised: September 24, 2020

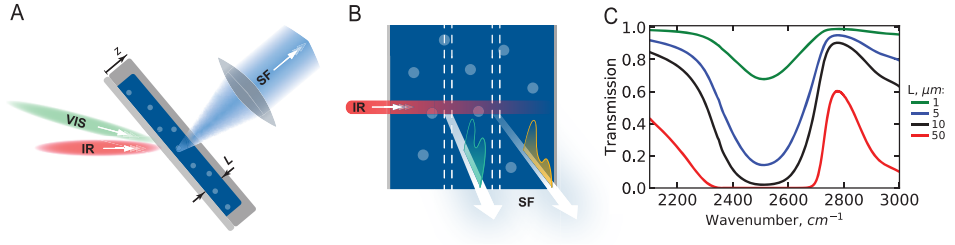

Figure 1. Linear optical interactions distort SFS spectra. (A) Sketch of the SFS experiment. The direction of the outgoing SF light is perpendicular to the cuvette and indicated as z. L is the thickness of the cuvette. (B) Illustration of linear IR absorption in an SFS experiment aimed to measure interfacial water in an aqueous medium. (C) IR transmission profiles for different slab thicknesses of a 1:1 D_2O:H_2O mixture.

dispersed in a hydrophobic liquid.[60] The inverse, the measurement of the vibrational water spectrum of an object dispersed in aqueous solution, has not been measured: Water spectra have only been measured up to the edges of the high-frequency side of the absorption band in D_2O[61] (from 2650−2750 cm^{-1}) and in a H_2O:D_2O mixture[62,63] (from 2600−2750 cm^{-1}), excluding the biggest part of the vibrational stretch mode region of water (2200−2750 cm^{-1} for D−O stretch modes).

Thus, even though a vibrational water spectrum of a nanoscale interface embedded in water would contain a wealth of information about interfacial water structure and hydrogen bonding interactions, it has not been measured. The reason for this lack of information is that water is a highly absorptive medium for infrared pulses. Therefore, it is expected to be very challenging to measure and interpret the SF scattering spectrum of particles, liposomes, or droplets dispersed in water. Figure 1B illustrates what happens to an IR pulse as it travels through water: After a distance in the order of a micrometer, the IR beam will be attenuated significantly as the IR light is absorbed by the water. This attenuation is frequency dependent, distorting the spectral contents of the IR light. Figure 1C shows IR transmission spectra of 1:1 mixtures of H_2O and D_2O for several different optical path lengths ranging from 1 to 50 μm. Taking D-O stretch modes as the vibrational modes of interest, for the strongest absorption at a frequency of ∼2500 cm^{-1}, after 10 μm penetration, all intensity is absorbed, while for ∼2750 cm^{-1} there is still >50% of the original intensity after 50 μm of path length. This means that as an IR pulse travels through an absorptive medium, such as water, its intensity attenuates drastically and its spectral shape is continuously modified. In order to understand vibrational SFS spectroscopy in an absorptive medium, a computational analysis is desirable.

Here, we describe a computational study of SF scattering of interfacial O-D vibrational stretch modes of a scattering object in an absorptive medium. The presented theory is valid when the probed surface is composed of the same chemicals as the bulk medium. We focus on the example of sub-micron-sized / nanoscale scattering objects (e.g., particles, droplets, bubbles, or liposomes) in an aqueous medium and calculate the vibrational SFS response of the interfacial water. We assume single scattering, valid for the experiments that have so far been published in the literature. We compute scattered SF spectra of the vibrational modes of interfacial water, given a certain defined surface response and determine the modulation of the surface optical response by absorption of the IR pulse. We then consider the effect of the presence of a nonresonant interfacial response and the size of the scattering volume, determined by optics that collects the generated SF photons and the linear scattering in the turbid medium. We find that IR absorption, a nonresonant background, and the choice of the scattering volume from which the SF light is detected can all drastically modify the spectral shape of the scattered SF light. For SFS experiments aimed at measuring interfacial structures of nano-objects dispersed in a strongly absorbing medium, our framework allows one to recognize artifacts and retrieve the true interfacial spectrum.

RESULTS AND DISCUSSION

Approach. In order to perform the computational analysis, we start with the expression for the SFS intensity that is emitted from a certain scattering volume.[64] For a sample with an optical path length L for the SF light, in the z-direction (Figure 1A), the intensity of scattered SF photons ($I_{SF}(\omega_{SF}; \omega_{VIS}, \omega_{IR})$) is given by:

$$I_{SF}(\omega_{SF}; \omega_{VIS}, \omega_{IR}) \propto \int_0^L |\Gamma^{(2)}(\omega_{SF}; \omega_{VIS}, \omega_{IR})|^2 I_{IR}(\omega_{IR}, z) I_{VIS}(\omega_{VIS}, z) f_{focal}(z)\rho(z)dz, \quad (1)$$

where ω_{SF}, ω_{VIS}, and ω_{IR} are the frequencies of the SF, VIS, and IR pulses, respectively, $I_{IR}(\omega_{IR}, z)$ is the intensity of the incident infrared illumination, $I_{VIS}(\omega_{VIS}, z)$ is the intensity of the incident visible illumination, $f_{focal}(z)$ is a collection function that describes the efficiency of light collection along the optical axis z of the collection optics, and $\rho(z)$ is the number density of particles at a specific depth. $\Gamma^{(2)}(\omega_{SF}; \omega_{VIS}, \omega_{IR})$ is the effective second-order particle susceptibility[65] that describes the spectral interfacial response of the object dispersed in the solution. $\Gamma^{(2)}(\omega_{SF}; \omega_{VIS}, \omega_{IR})$ is a function of the scattering angle (θ, defined as the angle between the scattered SF wavevector and that of the phase-matched direction), the size of the object (typically indicated by R, the radius), and the second-order surface susceptibility ($\chi^{(2)}$). Note that eq 1 is written in terms of second-order effects but can be expanded to include effective third-order processes.[48,49] Since the source of the interfacial response is not the topic of the present study, we will use a spectral function for $|\Gamma^{(2)}(\omega_{SF}; \omega_{VIS}, \omega_{IR})|^2 = |\Gamma^{(2)}|^2$ as input for eq 1. This means that the values of R, θ, and $\chi^{(2)}$ are not relevant here. Equation 1 can be solved by numerically computing the function under the integral for small dz distances (taken here as 1 μm), which are then summed. The optical distance L is taken to be 100 μm to resemble a typical sample cell used for SFS measurements.[64] The bulk medium is (somewhat arbitrarily) chosen to be a 1:1 mixture of light and heavy water as it is less absorptive than pure H_2O or D_2O.

https://dx.doi.org/10.1021/acs.jpcc.0c05196
J. Phys. Chem. C XXXX, XXX, XXX−XXX

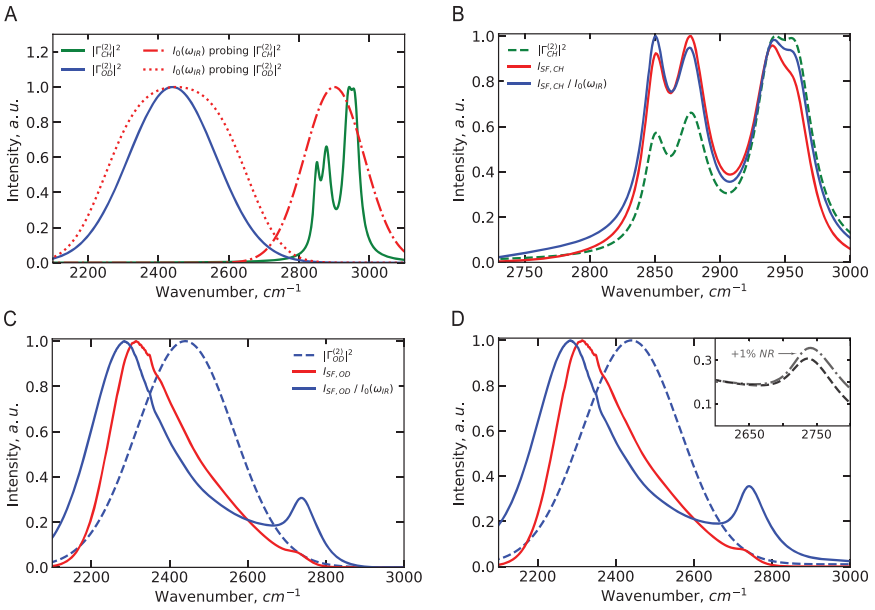

Figure 2. Effect of IR absorption. (A) Inputs used for $|\Gamma^{(2)}|^2$ and $I_0(\omega_{IR})$ in eq 1. The red lines represent the spectral shapes of the IR pulses ($I_0(\omega_{IR})$) used to probe the O−D (dotted line) and C−H (dashed−dotted line) stretch mode regions. The green curve represents $|\Gamma^{(2)}|^2$ for the C−H modes, and the blue curve represents $|\Gamma^{(2)}|^2$ for the O-D modes. (B) Effect of IR absorption on the model C−H band. The simulated signal (solid red line) is the resulting SF intensity that would be measured, and the solid blue line is the SF intensity divided by the spectral profile of the IR pulse. (C) Effect of IR absorption on the model O−D band. The simulated signal (solid red line) is the resulting SF intensity that would be measured, and the solid blue line is the SF intensity divided by the spectral profile of the IR pulse. (D) Effect of IR absorption on the model O-D band, including a nonresonant background. The nonresonant response is incorporated by adding a constant that has a magnitude of 1% of the maximum of the blue spectrum (blue dashed line). The simulated signal (solid red line) is the resulting SF intensity that would be measured, and the solid blue line is the SF intensity divided by the spectral profile of the IR pulse. The inset shows the amplifying influence of a nonresonant background on the high-frequency peak-like feature.

For the description of the surface response, we take an input function for $|\Gamma^{(2)}|^2$ which is a spectral response that is based on reported responses for planar aqueous interfaces in the literature,[66] since vibrational surface SF spectra of small objects dispersed in water have not yet been measured. In an actual experiment, $\Gamma^{(2)}$ is the physical quantity that one wants to retrieve. Here, we take a certain surface response and examine how the spectral shape of this response is modified by the linear optical interactions in the experiment. The chosen response is plotted as shown in Figure 2A and resembles a typical planar water SF surface spectrum in a 1:1 mixture of light and heavy water.[66] We model both C−H and O−D stretch modes and, for convenience, represent $|\Gamma^{(2)}|^2$ by Gaussians, for the O−D modes, and Lorentzians, for the C−H modes, centered in the O−D and C−H stretch regions, respectively, containing the most common features that are found in the SF spectral response from a typical aqueous interface. $|\Gamma^{(2)}|^2$ of the C−H modes (green curve, Figure 2A) is represented by 4 Lorentzians centered at 2850 cm^{-1} (with a full width at half maximum (FWHM) of 20 cm^{-1} and a relative amplitude of 0.3), 2878 cm^{-1} (with an FWHM of 30 cm^{-1} and a relative amplitude of 0.4), 2939 cm^{-1} (with an FWHM of 30 cm^{-1} and a relative amplitude of 0.5), and 2959 (with an FWHM of 30 cm^{-1} and a relative amplitude of 0.5). These modes represent the symmetric methylene stretch mode, the symmetric methyl stretch mode, the Fermi-resonance, and the asymmetric methyl stretch mode, respectively. $|\Gamma^{(2)}|^2$ of the O−D modes (blue curve, Figure 2A) is modeled by a broad Gaussian centered at 2450 cm^{-1} with an FWHM of 292 cm^{-1}. In the Supporting Information, we present a D_2O $|\Gamma^{(2)}|^2$ spectrum that is composed of three features that one finds regularly in the literature: Two broad modes at ∼2370 and ∼2510 cm^{-1} and one sharper feature at 2745 cm^{-1} (Figure S1A).[12,23,60] Note that the relative amplitude, width, and precise central frequencies of the O−D stretch peaks in an actual experiment are determined by the type of the interface. Since we are interested in the difference between the input spectral function and the output SF intensity, the actual choice of the explicit form of $|\Gamma^{(2)}|^2$ is not very important, as long as the spectrum contains spectral features that are characteristic of the substance. The effect of a nonresonant background is considered by adding a constant to the spectral response.

For measurements in a nonabsorptive medium, the observed SF signal is normalized by the intensities of IR and VIS beams incident on the sample, as has been described earlier.[55] In this case, eq 1 reverts to the familiar expression: $I_{SF}(\omega_{SF}; \omega_{VIS}, \omega_{IR}) \propto |\Gamma^{(2)}(\omega_{SF}; \omega_{VIS}, \omega_{IR})|^2 I_{IR}(\omega_{IR}) I_{VIS}(\omega_{VIS})$. For the visible beam ($I_{vis}$), there is an attenuation effect caused by linear light scattering, which was described earlier for second harmonic scattering[67] and SFS.[64] For this, we would have $I_{vis}(\omega_{vis}, z) = I_0(\omega_{vis})e^{-\tau_{vis}z}$ with τ_{vis} the turbidity. The same applies to the IR and SF beams. However, in what follows, we consider a small refractive index difference between the particles and the bulk medium (known as the Rayleigh−Gans−Debye approximation[51]), which means we neglect attenuation through linear scattering. This is appropriate since the effect of IR absorption is much bigger. For a typical 1 vol % sample of oil in water (100 nm radius droplets and 0.1 mm optical path length), the turbidity reduces the light intensity by <0.1% (as measured at a wavelength of 800 or 632 nm). For scattering by IR light, this would be further reduced since light scattering is more efficient for blue colors. For IR absorption at ∼2500 cm^{-1}, the IR light

https://dx.doi.org/10.1021/acs.jpcc.0c05196
J. Phys. Chem. C XXXX, XXX, XXX−XXX

is fully absorbed after ~10 microns for 100% D_2O, which means the difference in light attenuation between linear scattering and absorption is at least 3 orders of magnitude.

For the measurement of an interfacial water spectrum of particles dispersed in water, approximating $I_{IR}(\omega_{IR}, z)$ as the infrared pulse that is generated by the light source[64] is insufficient, as the IR spectral profile attenuates and changes drastically when the beam propagates through the sample (illustrated in Figure 1B). Therefore, the measured SF intensity cannot simply be normalized by the incident IR beam profile or an IR beam profile multiplied with the IR transmission spectrum. Instead, we have to take:

$$I_{IR}(\omega_{IR}, z) = I_0(\omega_{IR})e^{-\alpha(\omega_{IR})z} \quad (2)$$

where $I_{IR}(\omega, z)$ is the IR intensity at z, $I_0(\omega_{IR})$ is the incident intensity, and $\alpha(\omega_{IR})$ is the absorption spectrum. $\alpha(\omega_{IR})$ is computed from the measured IR transmission spectrum (T, Figure 1C black line) using Lambert−Beer's law, $\alpha(\omega_{IR}) = \frac{-\ln(T(\omega_{IR}))}{L}$. $T(\omega_{IR}, L = 10\ \mu m) = I_{IR}(\omega_{IR}, L = 10\ \mu m)/I_0(\omega_{IR}))$ of a 10 μm layer of a 1:1 D_2O:H_2O mixture with a spectrally flat $I_0(\omega_{IR})$. Figure S1 is computed using the transmission spectrum of 100% D_2O. In the experiments, $I_0(\omega_{IR})$ is not spectrally flat but composed of femtosecond broadband laser pulses. To model these, for probing C−H modes, we use a 200 cm^{-1} FWHM Gaussian, centered at 2900 cm^{-1} for $I_0(\omega_{IR})$. For the O−D modes, we use 4 Gaussians with 200 cm^{-1} FWHM centered at 2600, 2500, 2400, and 2300 added together for $I_0(\omega_{IR})$ to simulate an SFS experiment in which the bandwidth of a single IR pulse envelope is smaller than that of the O−D vibrational stretch band, as is the case in most experiments.[60] Both spectra are plotted in Figure 2A as the red dashed−dotted line and the red dotted line, respectively.

Equation 1 also contains the particle density as a function of penetration depth, which we consider as constant ($\rho(z) = \rho$), and the scattering volume, determined by the focal depth function of the collecting lens ($f_{focal}(z)$). We will initially assume that $f_{focal}(z) = 1$ for $0 < z < L$ and 0 elsewhere, meaning that we assume that the collection lens does not influence the experiment, and the scattered SF light that is generated at every point in the sample is detected. We will first consider the effect of absorption on the SFS result and then examine the effect of adding a nonresonant contribution. Finally, we will consider the effect of using a very small collection focal volume such as from an objective, or a somewhat larger one, such as from a small focal volume singlet lens.

Effect of IR Absorption. Having described our approach, we consider the results of the computation. First, we discuss the influence of the absorption of the IR pulse. Figure 2B shows the input function for $|\Gamma^{(2)}|^2$ (green curve) for the C−H modes. Computing eq 1 for this spectral region results in the simulated signal represented by the red line ($I_{SF, CH}$). This includes both multiplying by the spectral shape of the incoming pulses, $I_0(\omega_{IR})$, as well as correcting for IR absorption (eq 2). Both effects combined result in a spectral difference compared to the input $|\Gamma^{(2)}|^2$. It is common in the SFS literature[55] to report the measured intensity divided by the IR pulse spectrum ($I_{SF, CH}/I_0(\omega_{IR})$). This curve is shown as the blue line in Figure 2B. The additional effect of IR absorption by the H_2O/D_2O mixture changes the relative intensities of the C−H modes, even though the amount of IR absorption >2800 cm^{-1} is relatively low compared to that in the region 2200−2800 cm^{-1}. The amplitude ratios of the symmetric CH_2 and CH_3 stretch modes report on alkyl chain order,[41,68] and the amplitude ratios of the CH_3 symmetric and asymmetric stretch modes report on the alkyl chain tilt angle[69]. Both of these ratios could be influenced by absorption. For a 1:1 H_2O:D_2O mixture as a bulk medium, the difference in amplitude is 9 and 20%, respectively. This amounts to an approximate change in the tilt angle of <7°. Note that this estimation was made taking ratios of a recent study[58] and ignoring the fact that this study was conducted in pure D_2O. Thus, for this case, taking into account IR absorption is preferred but failing to do so will impose an additional error of ~10%, which might be acceptable depending on the aim of the study. For the case that the bulk medium is composed of 100% D_2O, computed spectra are given in Figure S1A. These data show that, in this case, there is a very small difference between the measured amplitude ratios with respect to the original ratios. In this case, a correction for IR absorption is not needed.

Figure 2C shows the $|\Gamma^{(2)}|^2$ input function for the surface response in the O−D stretch region as the blue dashed line. Using this function together with the IR pulse shown in Figure 2A (red dotted line) and the 1 μm IR absorption spectrum shown in Figure 1C, we compute the red line as $I_{SF, OD}$ using eq 1. It can be seen that this simulated spectrum differs significantly from the input: The main peak is shifted to lower frequencies, the spectral response is no longer symmetric, and at the high-frequency side, a distinct peak emerges. Processing this simulated equivalent of raw data by dividing it with the incident IR spectrum ($I_0(\omega_{IR})$), we obtain the blue curve. This processed spectrum has a completely different shape from the actual surface response ($|\Gamma^{(2)}|^2$, blue dashed line): The peak shifted to lower frequency (from 2500 to 2285 cm^{-1}), has an overall asymmetric peak shape, and there is a new peak-like feature at 2735 cm^{-1}. Using D_2O as the main medium and changing the spectrum to include three features instead of one, we reproduce the same result. Figure S1 shows the result of the same simulation used for $|\Gamma^{(2)}|^2$: an input spectrum with two broad features at ~2370 and ~ 2510 cm^{-1} (Figure S1B) and an additional sharper peak at 2745 cm^{-1} (Figure S1C, D) as observed at the planar D_2O/air,[66] oil/D_2O,[23,70] and D_2O water droplet in the oil SFS spectrum.[60] For the broad features, a shift to lower frequencies is observed. Without the feature at 2745 cm^{-1}, a new peak appears at ~2748 cm^{-1}, while with an already prominent feature at 2745 cm^{-1}, this peak is enhanced to ~10 x its original intensity.

Next, we examine the effect of including a nonresonant background in $|\Gamma^{(2)}|^2$. Many reported water spectra in the literature exhibit a nonresonant background. This background varies depending on the sample and sometimes on the way in which it is measured. For example, the water/air spectra recorded by various groups[10] show a nonresonant contribution of <3%. Tyrode and co-workers explicitly fitted the nonresonant background amplitude to ~1% with respect to the main peak.[14] The oil/water planar interface recorded by the Bakker lab shows a nonresonant contribution of ~3%,[23] while the Richmond lab reports a much lower value of ~0%.[22] Incorporating a nonresonant contribution that has a magnitude of 1% of the maximum response, we obtain the blue dashed line as shown in Figure 2D. Taking this as the surface response, $I_{SF, OD}$ is similar to the one shown in Figure 2C but with a more pronounced high-frequency peak. Dividing this spectrum by the incident IR radiation ($I_{SF, CH}/I_0(\omega_{IR})$), we obtain the blue curve which is similar in the low-frequency side to the one

https://dx.doi.org/10.1021/acs.jpcc.0c05196
J. Phys. Chem. C XXXX, XXX, XXX−XXX

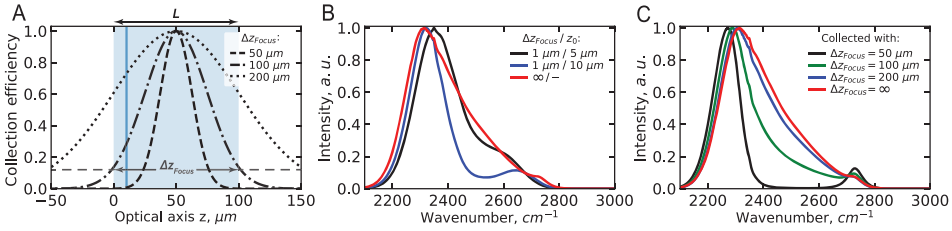

Figure 3. SF light collection. (A) Sketch of the sample cell (light blue), with the profiles of the different z−sectioning indicated: The vertical blue line represents a 1 μm thick slab, and the dashed, dot-dashed, and dotted lines represent lenses with different collection depths. (B) Comparison of collective SF signal obtained from two slabs both 1 μm thick but situated 5 μm deep (black) and 10 μm deep (blue) from the entrance window of the sample cuvette. (C) Comparison of collective SF signal obtained from the whole 100 μm sample with different lenses (depth of focus is changed as indicated in panel (A)). The red line is simulated assuming there is no difference in the collection efficiency across the sample (i.e., $f_{\text{focal}}(z) = 1$), or in other words representing a lens with an infinite depth of focus.

shown in Figure 2C but now has a more distinct broad peak riding on top of a rising slope (highlighted in the inset of Figure 2D).

Thus, linear absorption of IR excitation pulses will drastically modify the measured SFS spectrum such that it no longer agrees with the actual surface vibrational SF response. The ∼160 cm^{-1} shift of the main peak toward lower frequency would lead one to conclude that the interfacial structure of water is more ordered or even ice-like than it actually is. In addition to the changes to the hydrogen bond network, there is also the appearance of a high-frequency peak at 2735 cm^{-1}. This peak was not included in the original $|\Gamma^{(2)}|^2$ spectrum and is therefore an artifact produced by IR absorption. Thus, without using the full form of eq 1 to correct SFS spectra from absorptive media, one would misinterpret the surface structure. Had the result of the present simulation been measured in a real experiment, and without applying eq 1 in reverse, one might have concluded that the interfacial hydrogen bond network is much more strongly connected than it is in reality and that the interface would be populated by dangling O-D groups. Note that this does not apply to a sample of water droplets/ice particles dispersed in oil as reported in Ref.,[60] since the main phase is the oil phase and not the water. In this case, the considerations done here would apply to the vibrational modes of the oil phase.

Effect of the SF Light Scattering Volume. Next, we examine the effect of the scattering volume, determined by the collection lens and the turbid medium (Figure 1A). The light collection volume of the lens is determined by the specified focal length of the lens, together with the linear optical scattering properties of the dispersion. In eq 1, this combined effect is described by $f_{\text{focal}}(z)$, which quantifies the ability to collect SF light from different spots. The number of SF photons that are collected from a specific z-positon depends on how far this spot is located away from the geometrical focal point of the lens and what the effective focal distance of the lens is. Thus, the z-dependency of collection is convoluted with other depth-dependencies that are present in eq 1. For a nonabsorbing medium, the z-dependence of the collection optics does not play a big role since all scattering locations are illuminated with the same spectral profile. As a consequence, accounting for different collection efficiencies from different z-positions in the sample results in multiplying eq 1 by a constant. Spectral shapes or frequency distributions are not changed as a result. Therefore, thus far, SFS experiments from our laboratory have been performed with lenses that collect light from the entire optical path length of the sample (usually 100−1000 μm long, Refs.[45,64]). This strategy ensures that as many SF photons as possible are detected.

However, given that for an absorptive medium, the IR light will be attenuated after several microns (Figure 1C) and that this attenuation will be frequency-dependent, means that the spectral shape of the illuminating and scattered light will become z-dependent. It is therefore insightful to investigate the dependence of the emitted SF spectrum on the z-dependent intensity collection function $f_{\text{focal}}(z)$. One strategy of performing an experiment could be, instead of collecting all the emitted SF light, to collect only the light emitted from a thin slab just after the entrance window, since at this location, the IR spectrum is least distorted. Therefore, we investigate a few scenarios: (1) a collection z-range comprising a thin 1 μm wide slab, positioned at two different positions in the sample (illustrated as the dark blue line in Figure 3A), (2) a collection range with a wider Gaussian shape having three different widths (illustrated by the dashed lines in Figure 3A), and (3) the commonly employed scenario in which all scattered SF light is collected. Note that the collection lens is the determining factor for the scattering volume because of the beam geometry in a typical SFS experiment: The scattering geometry is selected such that the collection volume is smaller than the overlap volume of the IR and VIS beams to ensure a stable experiment. For example, a possible set of optics could be: 50 cm focusing lens for the VIS beam, 5 cm focusing parabolic mirror for the IR beam, and 1.8 cm collection lens for the SF signal. The collection volume can be fully enclosed within the IR focal volume, which in turn is enclosed within the visible focal volume. This type of experimental geometry has been employed to ensure uniform collection of the SF signal (as, for example, described in Ref.[64]).

The first scenario is achieved by setting $f_{\text{focal}}(z) = 1$ for $5 < z < 6$ μm and 0 elsewhere, and by setting $f_{\text{focal}}(z) = 1$ for $9 < z < 10$ μm and 0 elsewhere, representing two different locations close to and a little further away from the input window. For $|\Gamma^{(2)}|^2$, we assume the spectral response as shown Figure 2A (the blue line). Figure 3B shows the signal ($I_{\text{SF, OD}}$) collected from the entire sample region (same as the red line shown in Figure 2C, plotted here as the red line), a 1 μm thick z-slab placed 5 μm deep into the sample cell (black line), and a 1 μm thick z-slab placed 10 μm deep into the sample cell (blue line). Comparing the scenario where all scattered light is collected (red line) to the 1 μm thick z-slab placed 5 μm deep into the sample, a difference between the SF detected light is found, comprising a spectral shift on the low-frequency side and a different high-frequency shoulder on the high-frequency side.

https://dx.doi.org/10.1021/acs.jpcc.0c05196
J. Phys. Chem. C XXXX, XXX, XXX−XXX

The difference in spectral shape becomes more significant if the 1 μm slab is placed 10 μm deep into the sample cell (Figure 3B, blue line), resulting in an SF spectrum that seems to have two peaks rather than one. The difference between the two 1 μm z-slabs demonstrates that a small change in experimental parameters such as positioning of the collection lens can lead to dramatic changes in the detected spectral shape, even though the same interfacial response is detected. Although one could potentially calibrate the experiment for detecting the SF light from a narrow slab, given the z-sensitivity this strategy exposes one to unintentional errors.

Another option is to collect the intensity emitted from a wider range of sample depths, such as the ones shown in Figure 3A with a depth of focus (full width at $1/e^2$ of the maximum) of 50, 100, or 200 μm focused in the center of the sample cell, equivalent to using $f_{\text{focal}}(z) = e^{-(z-z_0)^2/\Delta z_{\text{focal}}^2}$ in eq 1. Figure 3C shows the computed spectra. The intensity from each slab is now additionally multiplied by individual collection coefficients defined by the collection profile of each lens (Figure 3A, dashed, dashed−dotted, and dotted lines). It can be seen that the smaller the collection volume, the more impacted the resulting spectrum is. For a narrow z-range placed in the middle of the sample cell (Δz_{focal}= 50 μm, black line), only the high- and low-frequency sides of the SF spectrum are collected as the IR absorption in these frequency ranges is less than that in the central spectral range. Broadening it, increasing Δz_{focal} to 200 μm (twice the width of the sample cell, blue line) results in a detected SF spectrum that is very close to the undistorted SF spectrum of the O-D modes. The above analysis, therefore, shows that choosing the widest possible collection volume (or z-range) is the best strategy for retrieving the most reliable surface SF spectrum from objects dispersed in water.

CONCLUSIONS

We have analyzed the effect of linear optical processes on the outcome of SF scattering measurements of particles dispersed in an adsorptive medium. In particular, for the case of water, we found that infrared absorption drastically modifies the interfacial (O−D) vibrational stretch spectral response. We used a model spectral response for the second-order particle susceptibility that resembles a common single wide spectral distribution for the O−D stretch modes (similar to the Raman spectrum). The emitted SF intensity is computed, taking into account IR absorption. The result of this computation, the simulated raw data of an SFS experiment are different from the original input spectrum: The main O−D stretch peak becomes asymmetric and is shifted to lower frequencies significantly (by ∼160 cm^{-1}), and a new peak-like feature appears in the high-frequency range of the spectrum. This peak-like feature is found to be more pronounced in the presence of a nonresonant background. We also found that these spectral distortions cannot be avoided by varying the light collection optics. Selectively collecting the spectrum from a thin slab close to the sample cell entrance window or using a lens with smaller collection volume can both result in distorted spectra with peaks shifted to lower frequencies, as well as in peak-like feature at high- and low-frequency spectral regions.

The simulations presented here illustrate that SF scattering measurements performed in any absorptive medium, and, in particular, water, are incomplete without appropriate correction procedures for linear optical effects. The approach used here to simulate the effect of IR absorption and changes in the scattering volume can also be used to correct actual data, provided that the scattering volume of the collecting lens is measured, as well as the infrared spectrum of the bulk medium. The presented computation provides the framework for correction routines that should be implemented in future vibrational SFS experiments involving absorptive bulk media. In detail, this involves applying eq 1 in reverse order:

$$|\Gamma^{(2)}(\omega_{\text{SF}}; \omega_{\text{VIS}}, \omega_{\text{IR}})|^2 \propto \frac{I_{\text{SF}}(\omega_{\text{SF}}; \omega_{\text{VIS}}, \omega_{\text{IR}})}{\int_0^L I_{\text{IR}}(\omega_{\text{IR}}, z) I_{\text{VIS}}(\omega_{\text{VIS}}, z) f_{\text{focal}}(z) \rho(z) \mathrm{d}z} \quad (3)$$

whereby the IR absorption and effects of the detection optics need to be included explicitly under the integral.

ASSOCIATED CONTENT

Supporting Information

The Supporting Information is available free of charge at https://pubs.acs.org/doi/10.1021/acs.jpcc.0c05196.

Figure with results for pure heavy water as a bulk medium, and corresponding discussion (PDF)

AUTHOR INFORMATION

Corresponding Author

Sylvie Roke − *Laboratory for fundamental BioPhotonics, Institutes of Bioengineering (IBI) and Materials Science (IMX) and Engineering, School of Engineering (STI), and Lausanne Centre for Ultrafast Science, École Polytechnique Fédérale de Lausanne (EPFL), CH-1015 Lausanne, Switzerland;* orcid.org/0000-0002-6062-7871; Email: sylvie.roke@epfl.ch

Authors

Sergey Kulik − *Laboratory for fundamental BioPhotonics, Institutes of Bioengineering (IBI) and Materials Science (IMX) and Engineering, School of Engineering (STI), and Lausanne Centre for Ultrafast Science, École Polytechnique Fédérale de Lausanne (EPFL), CH-1015 Lausanne, Switzerland*

Saranya Pullanchery − *Laboratory for fundamental BioPhotonics, Institutes of Bioengineering (IBI) and Materials Science (IMX) and Engineering, School of Engineering (STI), and Lausanne Centre for Ultrafast Science, École Polytechnique Fédérale de Lausanne (EPFL), CH-1015 Lausanne, Switzerland;* orcid.org/0000-0002-7011-0788

Complete contact information is available at: https://pubs.acs.org/10.1021/acs.jpcc.0c05196

Notes

The authors declare no competing financial interest.

ACKNOWLEDGMENTS

The authors thank Dr. Jerry I. Dadap for fruitful discussions. The authors also thank the Julia Jacobi Foundation and the Swiss National Science Foundation (grant numbers 200021-182606-1).

REFERENCES

(1) de Leeuw, G.; Andreas, E. L.; Anguelova, M. D.; Fairall, C. W.; Lewis, E. R.; O'Dowd, C.; Schulz, M.; Schwartz, S. E. Production Flux of Sea Spray Aerosol. *Rev. Geophys.* **2011**, *49*, 1−39.

(2) Prather, K. A.; et al. Bringing the Ocean into the Laboratory to Probe the Chemical Complexity of Sea Spray Aerosol. *P Natl Acad Sci USA* **2013**, *110*, 7550−7555.
(3) Zhang, M.; Wei, L. J.; Chen, H.; Du, Z. P.; Binks, B. P.; Yang, H. Q. Compartmentalized Droplets for Continuous Flow Liquid Liquid Interface Catalysis. *J. Am. Chem. Soc.* **2016**, *138*, 10173−10183.
(4) Ball, P. Water as an Active Constituent in Cell Biology. *Chem. Rev.* **2007**, *108*, 74−108.
(5) Zachara, J. M.; Moran, J. J.; Resch, C. T.; Lindemann, S. R.; Felmy, A. R.; Bowden, M. E.; Cory, A. B.; Fredrickson, J. K. Geo- and Biogeochemical Processes in a Heliothermal Hypersaline Lake. *Geochim Cosmochim Ac* **2016**, *181*, 144−163.
(6) Harris, A. L.; Chidsey, C. E. D.; Levinos, N. J.; Loiacono, D. N. Monolayer Vibrational Spectroscopy by Infrared-Visible Sum Generation at Metal and Semiconductor Surfaces. *Chem. Phys. Lett.* **1987**, *141*, 350−356.
(7) Hunt, J. H.; Guyot-Sionnest, P.; Shen, Y. R. Observation of C-H Stretch Vibrations of Monolayers of Molecules Optical Sum-Frequency Generation. *Chem. Phys. Lett.* **1987**, *133*, 189−192.
(8) Du, Q.; Superfine, R.; Freysz, E.; Shen, Y. R. Vibrational Spectroscopy of Water at the Vapor/Water Interface. *Phys.Rev.Lett.* **1993**, *70*, 2313−2316.
(9) Gopalakrishnan, S.; Liu, D. F.; Allen, H. C.; Kuo, M.; Shultz, M. J. Vibrational Spectroscopic Studies of Aqueous Interfaces: Salts, Acids, Bases, and Nanodrops. *Chem. Rev.* **2006**, *106*, 1155−1175.
(10) Feng, R.-r.; Guo, Y.; Lü, R.; Velarde, L.; Wang, H.-f. Consistency in the Sum Frequency Generation Intensity and Phase Vibrational Spectra of the Air/Neat Water Interface. *J. Phys. Chem. A.* **2011**, *115*, 6015−6027.
(11) Stiopkin, I. V.; Weeraman, C.; Pieniazek, P. A.; Shalhout, F. Y.; Skinner, J. L.; Benderskii, A. V. Hydrogen Bonding at the Water Surface Revealed by Isotopic Dilution Spectroscopy. *Nature* **2011**, *474*, 192−195.
(12) Bonn, M.; Nagata, Y.; Backus, E. H. G. Molecular Structure and Dynamics of Water at the Water−Air Interface Studied with Surface-Specific Vibrational Spectroscopy. *Angew. Chem., Int. Ed.* **2015**, *54*, 5560−5576.
(13) Mondal, S. K.; Inoue, K.; Yamaguchi, S.; Tahara, T. Anomalous Effective Polarity of an Air/Liquid-Mixture Interface: A Heterodyne-Detected Electronic and Vibrational Sum Frequency Generation Study. *Phys. Chem. Chem. Phys.* **2015**, *17*, 23720−23723.
(14) Sengupta, S.; Moberg, D. R.; Paesani, F.; Tyrode, E. Neat Water−Vapor Interface: Proton Continuum and the Nonresonant Background. *J. Phys. Chem. Lett.* **2018**, *9*, 6744−6749.
(15) Liu, J.; Conboy, J. C. Phase Transition of a Single Lipid Bilayer Measured by Sum-Frequency Vibrational Spectroscopy. *J. Am. Chem. Soc.* **2004**, *126*, 8894−8895.
(16) Gurau, M. C.; Kim, G.; Lim, S.-M.; Albertorio, F.; Fleisher, H. C.; Cremer, P. S. Organization of Water Layers at Hydrophilic Interfaces. *ChemPhysChem* **2003**, *4*, 1231−1233.
(17) Mondal, J. A.; Nihonyanagi, S.; Yamaguchi, S.; Tahara, T. Three Distinct Water Structures at a Zwitterionic Lipid/Water Interface Revealed by Heterodyne-Detected Vibrational Sum Frequency Generation. *J.Am.Chem.Soc.* **2012**, *134*, 7842−7850.
(18) Sung, W.; Kim, D.; Shen, Y. R. Sum-Frequency Vibrational Spectroscopic Studies of Langmuir Monolayers. *Curr. Appl. Phys.* **2013**, *13*, 619−632.
(19) Johnson, C. M.; Baldelli, S. Vibrational Sum Frequency Spectroscopy Studies of the Influence of Solutes and Phospholipids at Vapor/Water Interfaces Relevant to Biological and Environmental Systems. *Chem. Rev.* **2014**, *114*, 8416−8446.
(20) Roke, S.; Schins, J.; Muller, M.; Bonn, M. Vibrational Spectroscopic Investigation of the Phase Diagram of a Biomimetic Lipid Monolayer. *Phys. Rev. Lett.* **2003**, *90*, 128101.
(21) Scatena, L. F.; Brown, M. G.; Richmond, G. L. Water at Hydrophobic Surfaces: Weak Hydrogen Bonding and Strong Orientation Effects. *Science* **2001**, *292*, 908−912.
(22) Brown, M. G.; Walker, D. S.; Raymond, E. A.; Richmond, G. L. Vibrational Sum-Frequency Spectroscopy of Akane/Water Interfaces: Experiment and Theoretical Simulation. *J. Phys. Chem. B* **2003**, *107*, 237−244.
(23) Strazdaite, S.; Versluis, J.; Backus, E. H. G.; Bakker, H. J. Enhanced Ordering of Water at Hydrophobic Surfaces. *J. Chem. Phys.* **2014**, *140*, No. 054711.
(24) Strazdaite, S.; Versluis, J.; Bakker, H. J. Water Orientation at Hydrophobic Interfaces. *J. Chem. Phys.* **2015**, *143*, No. 084708.
(25) Wang, J.; Chen, X. Y.; Clarke, M. L.; Chen, Z. Detection of Chiral Sum Frequency Generation Vibrational Spectra of Proteins and Peptides at Interfaces in Situ. *Proc. Natl. Acad. Sci. U. S. A.* **2005**, *102*, 4978−4983.
(26) Chen, C. Y.; Clarke, M. L.; Wang, J.; Chen, Z. Comparison of Surface Structures of Poly(Ethyl Methacrylate) and Poly(Ethyl Acrylate) in Different Chemical Environments. *Phys. Chem. Chem. Phys.* **2005**, *7*, 2357−2363.
(27) Gurau, M. C.; Lim, S. M.; Castellana, E. T.; Albertorio, F.; Kataoka, S.; Cremer, P. S. On the Mechanism of the Hofmeister Effect. *J. Am. Chem. Soc.* **2004**, *126*, 10522−10523.
(28) Zhang, Y. J.; Cremer, P. S. Interactions between Macromolecules and Ions: The Hofmeister Series. *Curr. Opin. Chem. Biol.* **2006**, *10*, 658−663.
(29) Fu, L.; Liu, J.; Yan, E. C. Y. Chiral Sum Frequency Generation Spectroscopy for Characterizing Protein Secondary Structures at Interfaces. *J. Am. Chem. Soc.* **2011**, *133*, 8094−8097.
(30) Gibbs-Davis, J. M.; Kruk, J. J.; Konek, C. T.; Scheidt, K. A.; Geiger, F. M. Jammed Acid-Base Reactions at Interfaces. *J. Am. Chem. Soc.* **2008**, *130*, 15444−15447.
(31) Jena, K. C.; Covert, P. A.; Hore, D. K. The Effect of Salt on the Water Structure at a Charged Solid Surface: Differentiating Second- and Third-Order Nonlinear Contributions. *J. Phys. Chem. Lett.* **2011**, *2*, 1056−1061.
(32) Azam, M. S.; Cai, C. Y.; Gibbs, J. M.; Tyrode, E.; Hore, D. K. Silica Surface Charge Enhancement at Elevated Temperatures Revealed by Interfacial Water Signals. *J. Am. Chem. Soc.* **2020**, *142*, 669−673.
(33) Du, Q.; Freysz, E.; Shen, Y. R. Vibrational Spectra of Water Molecules at Quartz/Water Interfaces. *Phys.Rev.Lett.* **1994**, *72*, 238−241.
(34) Bain, C. D. Sum-Frequency Vibrational Spectroscopy of the Solid-Liquid Interface. *J Chem Soc Faraday T* **1995**, *91*, 1281−1296.
(35) Baldelli, S.; Mailhot, G.; Ross, P. N.; Somorjai, G. A. Potential-Dependent Vibrational Spectroscopy of Solvent Molecules at the Pt(111) Electrode in a Water/Acetonitrile Mixture Studied by Sum Frequency Generation. *J. Am. Chem. Soc.* **2001**, *123*, 7697−7702.
(36) Tong, Y. J.; Lapointe, F.; Thamer, M.; Wolf, M.; Campen, R. K. Hydrophobic Water Probed Experimentally at the Gold Electrode/Aqueous Interface. *Angew. Chem., Int. Ed.* **2017**, *56*, 4211−4214.
(37) Yan, E. C. Y.; Fu, L.; Wang, Z. G.; Liu, W. Biological Macromolecules at Interfaces Probed by Chiral Vibrational Sum Frequency Generation Spectroscopy. *Chem. Rev.* **2014**, *114*, 8471−8498.
(38) Shen, Y. R. Surfaces Probed by Nonlinear Optics. *Surf. Sci.* **1994**, *299-300*, 551−562.
(39) Eisenthal, K. B. Liquid Interfaces Probed by Second-Harmonic and Sum-Frequency Spectroscopy. *Chem. Rev.* **1996**, *96*, 1343−1360.
(40) Richmond, G. L. Structure and Bonding of Molecules at Aqueous Surfaces. *Annu. Rev. Phys. Chem.* **2001**, *52*, 357−389.
(41) Wang, H.-F.; Gan, W.; Lu, R.; Rao, Y.; Wu, B.-H. Quantitative Spectral and Orientational Analysis in Surface Sum Frequency Generation Vibrational Spectroscopy (Sfg-Vs). *Int. Rev. Phys. Chem.* **2005**, *24*, 191−256.
(42) Geiger, F. M. Second Harmonic Generation, Sum Frequency Generation, and Chi((3)): Dissecting Environmental Interfaces with a Nonlinear Optical Swiss Army Knife. *Annu. Rev. Phys. Chem.* **2009**, *60*, 61−83.
(43) Roke, S. Nonlinear Optical Spectroscopy of Soft Matter Interfaces. *ChemPhysChem* **2009**, *10*, 1380−1388.

https://dx.doi.org/10.1021/acs.jpcc.0c05196
J. Phys. Chem. C XXXX, XXX, XXX−XXX

(44) Roy, S.; Covert, P. A.; FitzGerald, W. R.; Hore, D. K. Biomolecular Structure at Solid-Liquid Interfaces as Revealed by Nonlinear Optical Spectroscopy. *Chem. Rev.* **2014**, *114*, 8388−8415.
(45) Roke, S.; Roeterdink, W. G.; Wijnhoven, J. E. G. J.; Petukhov, A. V.; Kleyn, A. W.; Bonn, M. Vibrational Sum Frequency Scattering from a Submicron Suspension. *Phys. Rev. Lett.* **2003**, *91*, 258302.
(46) Roke, S.; Gonella, G. Nonlinear Light Scattering and Spectroscopy of Particles and Droplets in Liquids. *Annu. Rev. Phys. Chem.* **2012**, *63*, 353−378.
(47) de Beer, A. G. F.; Roke, S. Obtaining Molecular Orientation from Second Harmonic and Sum Frequency Scattering Experiments in Water: Angular Distribution and Polarization Dependence. *J. Chem. Phys.* **2010**, *132*, 234702.
(48) de Beer, A. G. F.; Campen, R. K.; Roke, S. Separating Surface Structure and Surface Charge with Second-Harmonic and Sum-Frequency Scattering. *Phys. Rev. B* **2010**, *82*, 235431.
(49) Gonella, G.; Lütgebaucks, C.; de Beer, A. G. F.; Roke, S. Second Harmonic and Sum-Frequency Generation from Aqueous Interfaces Is Modulated by Interference. *J. Phys. Chem. C* **2016**, *120*, 9165−9173.
(50) Dadap, J. I.; de Aguiar, H. B.; Roke, S. Nonlinear Light Scattering from Clusters and Single Particles. *J Chem Phys* **2009**, *130*, 214710.
(51) de Beer, A. G. F.; Roke, S. Sum Frequency Generation Scattering from the Interface of an Isotropic Particle: Geometrical and Chiral Effects. *Phys. Rev. B* **2007**, *75*, 245438.
(52) Roke, S.; Buitenhuis, J.; van Miltenburg, J. C.; Bonn, M.; van Blaaderen, A. Interface-Solvent Effects During Colloidal Phase Transitions. *J Phys-Condens Mat* **2005**, *17*, S3469−S3479.
(53) Roke, S.; Berg, O.; Buitenhuis, J.; van Blaaderen, A.; Bonn, M. Surface Molecular View of Colloidal Gelation. *P Natl Acad Sci USA* **2006**, *103*, 13310−13314.
(54) de Aguiar, H. B.; de Beer, A. G. F.; Strader, M. L.; Roke, S. The Interfacial Tension of Nanoscopic Oil Droplets in Water Is Hardly Affected by Sds Surfactant. *J. Am. Chem. Soc.* **2010**, *132*, 2122.
(55) de Aguiar, H. B.; Strader, M. L.; de Beer, A. G. F.; Roke, S. Surface Structure of Sodium Dodecyl Sulfate Surfactant and Oil at the Oil-in-Water Droplet Liquid/Liquid Interface: A Manifestation of a Nonequilibrium Surface State. *J. Phys. Chem. B* **2011**, *115*, 2970−2978.
(56) Hensel, J. K.; Carpenter, A. P.; Ciszewski, R. K.; Schabes, B. K.; Kittredge, C. T.; Moore, F. G.; Richmond, G. L. Molecular Characterization of Water and Surfactant Aot at Nanoemulsion Surfaces. *P Natl Acad Sci USA* **2017**, *114*, 13351−13356.
(57) Johansson, P. K.; Koelsch, P. Vibrational Sum-Frequency Scattering for Detailed Studies of Collagen Fibers in Aqueous Environments. *J. Am. Chem. Soc.* **2014**, *136*, 13598−13601.
(58) Chen, Y.; Jena, K. C.; Lütgebaucks, C.; Okur, H. I.; Roke, S. Three Dimensional Nano "Langmuir Trough" for Lipid Studies. *Nano Lett.* **2015**, *15*, 5558−5563.
(59) Zdrali, E.; Baer, M. D.; Okur, H. I.; Mundy, C. J.; Roke, S. The Diverse Nature of Ion Speciation at the Nanoscale Hydrophobic/Water Interface. *J. Phys. Chem. B* **2019**, *123*, 2414−2423.
(60) Smolentsev, N.; Smit, W. J.; Bakker, H. J.; Roke, S. The Interfacial Structure of Water Droplets in a Hydrophobic Liquid. *Nat. Commun.* **2017**, *8*, 15548.
(61) Samson, J.-S.; Scheu, R.; Smolentsev, N.; Rick, S. W.; Roke, S. Sum Frequency Spectroscopy of the Hydrophobic Nanodroplet/Water Interface: Absence of Hydroxyl Ion and Dangling Oh Bond Signatures. *Chem. Phys. Lett.* **2014**, *615*, 124−131.
(62) Carpenter, A. P.; Tran, E.; Altman, R. M.; Richmond, G. L. Formation and Surface-Stabilizing Contributions to Bare Nanoemulsions Created with Negligible Surface Charge. *Proc. Natl. Acad. Sci. U. S. A.* **2019**, *116*, 9214.
(63) Carpenter, A. P.; Altman, R. M.; Tran, E.; Richmond, G. L. How Low Can You Go? Molecular Details of Low-Charge Nanoemulsion Surfaces. *J. Phys. Chem. B* **2020**, *124*, 4234−4245.
(64) de Aguiar, H. B.; Samson, J.-S.; Roke, S. Probing Nanoscopic Droplet Interfaces in Aqueous Solution with Vibrational Sum-Frequency Scattering: A Study of the Effects of Path Length, Droplet Density and Pulse Energy. *Chem. Phys. Lett.* **2011**, *512*, 76−80.
(65) Roke, S.; Bonn, M.; Petukhov, A. V. Nonlinear Optical Scattering: The Concept of Effective Susceptibility. *Phys. Rev. B* **2004**, *70*, 115106.
(66) Sovago, M.; Campen, R. K.; Wurpel, G. W. H.; Müller, M.; Bakker, H. J.; Bonn, M. Vibrational Response of Hydrogen-Bonded Interfacial Water Is Dominated by Intramolecular Coupling. *Phys. Rev. Lett.* **2008**, *100*, 173901.
(67) Schneider, L.; Schmid, H. J.; Peukert, W. Influence of Particle Size and Concentration on the Second-Harmonic Signal Generated at Colloidal Surfaces. *Appl. Phys. B: Lasers Opt.* **2007**, *87*, 333−339.
(68) Hirose, C.; Yamamoto, H.; Akamatsu, N.; Domen, K. Orientation Analysis by Simulation of Vibrational Sum-Frequency Generation Spectrum - Ch Stretching Bands of the Methyl-Group. *J. Phys. Chem.-Us* **1993**, *97*, 10064−10069.
(69) Tyrode, E.; Liljeblad, J. F. D. Water Structure Next to Ordered and Disordered Hydrophobic Silane Monolayers: A Vibrational Sum Frequency Spectroscopy Study. *J. Phys. Chem. C* **2013**, *117*, 1780−1790.
(70) Scatena, L. F.; Richmond, G. L. Orientation, Hydrogen Bonding, and Penetration of Water at the Organic/Water Interface. *J. Phys. Chem. B* **2001**, *105*, 11240−11250.

https://dx.doi.org/10.1021/acs.jpcc.0c05196
J. Phys. Chem. C XXXX, XXX, XXX−XXX